Plasmon-Mediated Synthesis of Hybrid Silver-Platinum Nanostructures

Abrar Habib,[†,§] Melissa E. King,[†,§] Leila L. Etemad,[†] Max E. Distler,[†] Katherine H. Morrissey,[‡] and Michelle L. Personick[†]*

[†] Department of Chemistry, Wesleyan University, Middletown, Connecticut 06459, United States

[‡] Valley Regional High School, Deep River, Connecticut 06417, United States

ABSTRACT: Fine tuning of metal ion reduction kinetics is crucial to the successful synthesis of designer bimetallic nanomaterials with well-defined morphologies and tailored localization of the constituent elements for use in catalysis, sensing, and other applications. However, achieving desired reduction kinetics can be challenging within the restrictions of available reducing agents, seed particle stability, metal ion solubility, and competing chemical processes such as galvanic exchange. Herein, we report the plasmon-assisted reduction of Pt ions onto Ag cores by using visible light illumination to accelerate the oxidation kinetics of a weak reducing agent, trisodium citrate. Using this approach, we are able to synthesize both core-shell and core-satellite structures composed of a plasmonic Ag core and a poorly plasmonic Pt shell or satellites. The controlled formation of these hybrid structures relies on the plasmon-mediated enhancement of the Pt ion reduction rate into a range where, under standard thermal conditions, reduction with citrate is too slow and reduction using even low concentrations of a slightly stronger reducing agent is too fast. This work expands the scope of citrate-assisted plasmon-mediated synthesis to metals other than Ag, opening possibilities for using plasmon-enhanced reduction by citrate as a more generalizable synthetic tool.

Introduction

The synthesis of well-defined bimetallic nanoparticles, whether alloyed, intermetallic, core-shell, or core-satellite, presents numerous challenges resulting from differing metal ion precursor chemistry and materials parameters.[1-3] For example, differences in lattice parameters or one metal having a high cohesive energy can lead to segregation and island formation.[4-7] Differences in reduction potential or reduction kinetics between two metal ion precursors can make it challenging to find a single reducing agent to reduce both precursors at appropriate relative rates to enable the formation of desired structures with intended compositions.[8] Two-step seed-mediated and co-reduction approaches can be employed to overcome some of these challenges when a core-shell or core-satellite structure is desired,[9, 10] though appropriate reducing conditions must still be identified to ensure deposition of the second metal occurs either conformally or at specific locations, as intended.

A particular challenge arises when the shell or satellite metal has a higher reduction potential than the core metal because ions of the second metal can oxidize atoms of the core metal. This process, known as galvanic exchange or galvanic replacement, often generates hollow or partially hollow structures due to the stoichiometry of the reaction, especially for silver (Ag) cores (+1 ion charge) with higher valent metals such as gold (Au^{3+}) or palladium (Pd^{2+}).[11-13] When well-controlled, galvanic replacement can yield structures ranging from exotic bimetallic morphologies with complex voids to simple epitaxial monolayers of a second metal.[6, 14-17] However, reducing agents must be carefully selected to balance direct reduction against desired or undesired galvanic exchange processes when designing bimetallic nanostructures with less noble cores, such as Ag and copper.[18, 19]

The synthesis of core-satellite structures with islands at designated sites of high chemical reactivity or strong plasmonic enhancement requires especially fine control of metal ion reduction.[20, 21] The strength of many common reducing agents used in metal nanoparticle synthesis can be increased (or decreased) by raising (or lowering) the reaction pH or temperature, or the reduction rate can be accelerated by selecting a metal ion precursor with a higher reduction potential. However, many of these parameters for increasing reduction rate also increase the rate of galvanic exchange. For deposition of Pt on Ag cores, for example, raising the reaction temperature or the reduction potential of the Pt precursor will also concomitantly increase the rate of undesired galvanic exchange, where Pt ions are reduced at the expense of oxidizing multiple Ag atoms to Ag^{+}, generating hollow voids and/or structural rearrangements.[12] Modification of pH is possible within a range, but even a strongly basic pH may be insufficient to increase reducing strength to an appropriate level and may lead to the formation of insoluble hydroxides and oxides.[22] Alternatively, lowering the pH to temper the reducing strength of a stronger reducing agent can lead to etching and instability when depositing a secondary metal onto Ag cores.

Plasmon-mediated nanoparticle synthesis provides an alternative, non-thermal means for influencing nanoparticle

growth kinetics by using low-intensity visible light to drive metal ion reduction.[23] The first reported plasmon-mediated synthesis for noble metal nanoparticles was a method for generating Ag triangular nanoprisms.[24] While the exact mechanism is somewhat debated, it is commonly accepted that excitation of the localized surface plasmon resonance (LSPR) of Ag seeds accelerates the kinetically slow oxidation of the weak reducing agent, trisodium citrate, thereby driving a redox cycle that leads to Ag ion reduction and nanoparticle growth.[25, 26] This result opened up new prospects for using the properties of light, such as wavelength and intensity, as additional handles with which to tune metal ion reduction rate in combination with traditional chemical parameters such as concentration and pH.[23]

For fifteen years, the field of plasmon-mediated noble metal nanoparticle synthesis was limited to the plasmon-mediated reduction of Ag, either in monometallic Ag nanoparticles or in Au core-Ag shell nanostructures.[23] Recently, there have been a few reports of plasmon-mediated syntheses of Au nanoprisms, in which the chemical composition of the nanoparticle growth solution is modified slightly to facilitate light-assisted growth of Au.[27, 28] In this case, methanol serves as a hole scavenger while polyvinylpyrrolidone functions to assist nanoprism formation.[27] Plasmonic excitation has also been used to directly reduce Pt ions onto Au nanorods with excited hot electrons,[29-31] as well as to reduce a Pt oxide layer that had been pre-deposited on Ag via galvanic exchange.[32] However, the original plasmon-mediated synthesis via the plasmonic photoreduction of citrate remains exclusive to Ag nanostructure formation.

The ability to use light to enhance the reducing ability of a weaker reducing agent, such as citrate, provides an avenue toward controllable nanomaterials synthesis in the chemical range where citrate would normally be too weak of a reducing agent, while even low concentrations of a slightly more powerful reducing agent, such as ascorbic acid, are too strong. We report the plasmon-mediated synthesis of Ag-Pt hybrid plasmonic/poorly-plasmonic nanostructures by using visible light excitation of Ag right triangular bipyramid cores to drive the photo-oxidation of citrate, which in turn provides electrons to reduce Pt ions. The rate of Pt ion reduction is controllable using both chemical parameters—such as Pt ion and citrate concentrations—and illumination parameters—such as wavelength and intensity. With careful tuning of reaction kinetics, we successfully synthesize core-satellite structures with Pt spheres localized at the tips of the Ag bipyramid cores, as well as other morphologies, such as core-shell structures. To our knowledge, this is the first example of the extension of the classic citrate-assisted plasmon-mediated synthesis to the reduction of a metal other than Ag.

Methods

Chemicals. Silver nitrate ($AgNO_3$, 99.9999% trace metals basis), sodium tetrachloroplatinate (II) hydrate ($Na_2PtCl_4 \bullet xH_2O$), and sodium borohydride ($NaBH_4$, granular, 99.99% trace metals basis) were purchased from Sigma-Aldrich. Bis(p-sulfonatophenyl)phenylphosphine dihydrate dipotassium salt (BSPP, $C_6H_5P(C_6H_4SO_3K)_2 \bullet 2H_2O$, min. 97%) was purchased from Strem Chemicals. Trisodium citrate dihydrate (citrate, $Na_3C_6H_5O_7$, ACS, 99.0% min.) and sodium hydroxide (NaOH, beads/pellets, 99.99% metals basis) were purchased from Alfa Aesar. Hydrochloric acid (HCl, TraceMetal™ grade) and nitric acid (HNO_3, Trace-Metal™ grade) were purchased from Fisher Scientific. Deionized (DI) water with a resistivity of 18.2 MΩ (Labconco Water Pro PS) was used to prepare all solutions and all chemicals were used without further purification.

Synthesis of Ag Right Triangular Bipyramids. Ag right triangular bipyramids were synthesized according to a previously reported method with minor modifications to improve structural quality and uniformity.[22] First, planar-twinned Ag seeds were synthesized according to a literature approach.[22] These seeds were stable for months when stored under refrigeration in the dark. In a subsequent step, DI water (17.9 mL), $AgNO_3$ (0.7 mL, 10 mM), BSPP (0.7 mL, 10 mM), trisodium citrate (0.3 mL, 100 mM), the planar-twinned Ag seeds (0.5 mL), and sodium hydroxide (0.9 mL, 100 mM) were mixed in a 22 mL glass vial with a Teflon septa cap (Thermo Scientific EPA screw vial). The final volume of the growth solution was 21 mL. The growth solution was then irradiated using a 150 W halogen lamp (Dolan-Jenner Fiber-Lite MI-150) in combination with a bandpass filter (550 ± 20 nm, Intor, 25 mm diameter). The power of the lamp was set to 0.15 W, measured at the light source by a photodiode power sensor (Thorlabs, S121C, 9.5 mm aperture diameter). The reaction vial was positioned horizontally with the bandpass filter directly against the bottom of the vial and a 1 cm distance between the bottom of the vial/filter and the lamp. At the base of the vial, the measured power was 75% of the power at the light source, and the illumination area was 4.91 cm^2. Prior to illumination, the sides of the vial were wrapped in foil to block out other light and immobilize the bandpass filter. The growth solution was illuminated overnight.

Synthesis of Ag-Pt Hybrid Nanoparticles. After overnight illumination, a 15 mL aliquot of the as-synthesized Ag bipyramids was transferred to a 15 ml conical tube and centrifuged for 10 min at 7830 RPM to isolate the bipyramids from residual reactants. After the particles were spun down, the supernatant was removed and the bipyramids were resuspended in 1.6 mL of DI water. The purified Ag bipyramids were combined with trisodium citrate (0.1-1.0 mL, 100 mM), Na_2PtCl_4 (25-100 µL, 10 mM), and enough DI water to bring the total volume to 21 mL in a 22 mL glass vial with a Teflon septa cap. (Note: the Na_2PtCl_4 solution was prepared using the anhydrous molecular weight.) In a standard reaction, the vial was then irradiated at 550 nm and a power of 0.1 W using the same setup as described above. Non-standard illumination conditions are described in the main text. The growth solution was illuminated for three hours and then removed from the light.

Synthesis of Ag Triangular Prisms. To synthesize large Ag triangular prisms, DI water (19.0 mL), $AgNO_3$ (0.6 mL, 10 mM), BSPP (0.6 mL, 10 mM), trisodium citrate (0.3 mL, 100 mM), and planar-twinned Ag seeds (0.5 mL) were mixed in a 22 mL glass vial with a Teflon septa cap. The vial was then irradiated at 550 nm and a power of 0.19 W overnight using the same setup as described above. To synthesize small Ag triangular prisms, DI water (18.875 mL), $AgNO_3$ (0.6 mL, 10 mM), BSPP (0.6 mL, 17.5 mM), trisodium citrate (0.3 mL, 100 mM), NaOH (0.125 mL, 100 mM) and planar-twinned Ag seeds (0.5 mL) were mixed in a 22 mL glass vial with a

Teflon septa cap. The vial was then irradiated at 550 nm and a power of 0.19 W overnight using the same setup as described above.

Instrumentation. Scanning electron microscopy (SEM) imaging was carried out using Hitachi SU-70 and SU-5000 field emission microscopes. Scanning transmission electron microscopy energy dispersive X-ray spectroscopy (STEM-EDS) imaging and mapping was conducted using a FEI Tecnai Osiris 200 kV TEM. Nanoparticle samples for SEM and STEM imaging were prepared by centrifuging a 0.5-1.0 mL aliquot of the reaction solution at 6,000 RPM for four minutes, washing the isolated particles with DI water to remove any excess reagents, and then centrifuging and resuspending the washed particles in 100 μL of DI water. The washed particles were drop-cast onto a slice of silicon wafer (for SEM) or formvar/carbon-coated copper grids (for STEM-EDS) and allowed to air dry.

Inductively coupled plasma mass spectrometry (ICP-MS) quantification of Pt content was carried out using a Perkin Elmer Elan DRC-e ICP-MS. To prepare samples for ICP-MS analysis, a 0.5 mL aliquot of the reaction solution was taken at different time points and immediately centrifuged for 10 min at 14,800 RPM to isolate the nanoparticles. The supernatant was removed, the particles were resuspended in 0.5 mL of DI water to wash away unreacted Pt ions and citrate, and the sample was again centrifuged for 10 min at the same rate. The supernatant was removed and the purified nanoparticles were resuspended in 0.5 mL of DI water and transferred to a 15 mL conical tube. The particles were then dissolved in 2.0 mL of aqua regia (3:1 HCl: HNO_3, **CAUTION: strong acid.**) Prior to ICP-MS analysis, the solution was diluted to a total volume of 5.0 mL with 2.5 mL of DI water. Triplicate measurements originate from three separate reactions. UV-visible spectra were collected using an Agilent Cary 100 UV-visible spectrophotometer.

Results and Discussion

Ag right bipyramid cores were synthesized according to a previously reported approach with slight modifications to improve shape and size monodispersity (Figure S1).[22, 33] In a standard synthesis of Ag-Pt hybrid nanostructures, 15.0 mL of as-synthesized Ag right bipyramids were centrifuged at 7830 RPM for 10 minutes. The supernatant was then discarded to remove residual reagents from the Ag bipyramid synthesis and the bipyramids were resuspended in 1.6 mL of water. These resuspended particles were combined in a 22 mL glass scintillation vial with Na_2PtCl_4 (25-150 μL, 10 mM) and trisodium citrate (0.1-1.0 mL, 100 mM) in enough DI water to bring the total volume to 21.0 mL. The vial containing the growth solution was shaken to mix the reagents and then immediately irradiated for three hours using a halogen lamp with a bandpass filter centered at a wavelength of 550 nm and a power of 0.1W, unless otherwise specified. The deposition of Pt onto the Ag cores is accompanied by a color change from pink to purple, blue, or teal, depending on the amount of Pt deposited (Figure S2A).

At room temperature, the reduction of Pt^{2+} by citrate is thermodynamically feasible based on redox potentials but it is kinetically slow, and Pt deposition in this synthesis proceeds via a plasmon-assisted mechanism. Plasmon-mediated syntheses take advantage of the plasmonic properties of Ag and Au nanoparticles to overcome this kinetic barrier.[23] The excitation of the LSPR of the core Ag bipyramids generates hot electrons and hot holes. Analogous to the plasmon-mediated synthesis of Ag nanoparticles, the hot holes irreducibly photo-oxidize surface-adsorbed citrate molecules to 1,3-acetonedicarboxylate and carbon dioxide, and the resulting electrons from this oxidation reaction are transferred to the Ag nanoparticle.[25, 26] These thermalized electrons then reduce Pt^{2+} ions to Pt^0 at the nanoparticle surface, facilitating Pt deposition. Unlike hot electrons that have lifetimes on the order of femtoseconds, the electrons that result from plasmon-assisted oxidation of citrate have been shown to be long lived and able to move throughout the nanoparticle.[25] Consequently, the location of metal deposition in plasmon-mediated nanoparticle synthesis is controlled by reaction kinetics and is not limited to sites of high electric field density.[23]

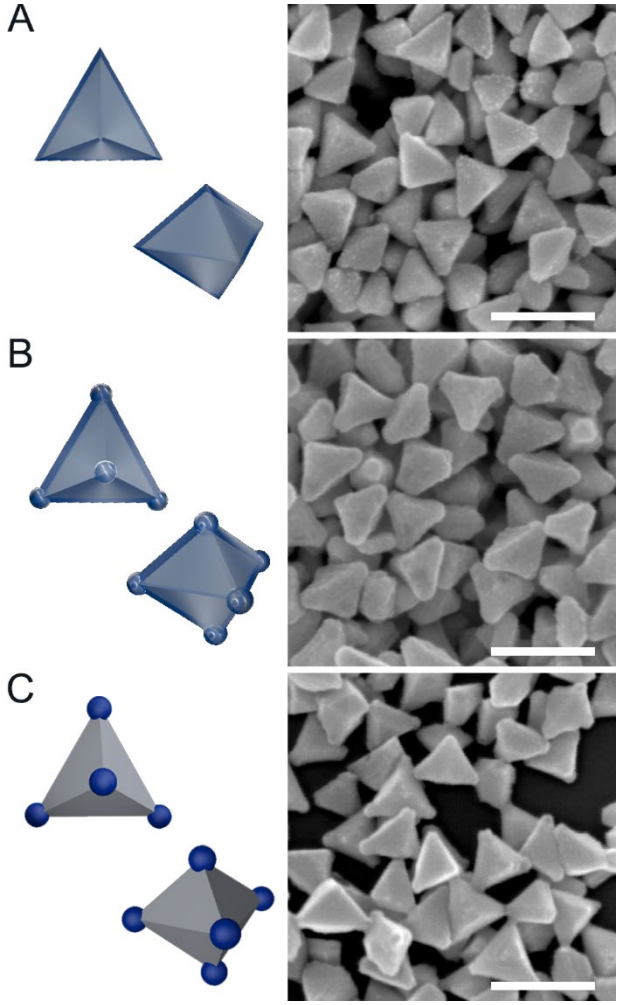

Figure 1. Models (left) and scanning electron microscopy (SEM) images (right) of Ag-Pt hybrid nanoparticles highlighting the following Pt growth modes: (A) thin shell formation; (B) thick shell formation with spherical protrusions at the bipyramid tips; (C) isolated growth of spheres at the bipyramid tips. The Ag-Pt hybrids were synthesized under the following conditions: (A) 23.8 μM Pt^{2+}, 4.76 mM citrate, three hours illumination; (B) 71.4 μM Pt^{2+}, 4.76 mM citrate, twenty hours illumination; and (C) 47.6 μM Pt^{2+}, 0.95 mM citrate, three hours illumination. All reactions were illuminated at 550 nm and 0.1 W. Scale bars: 200 nm.

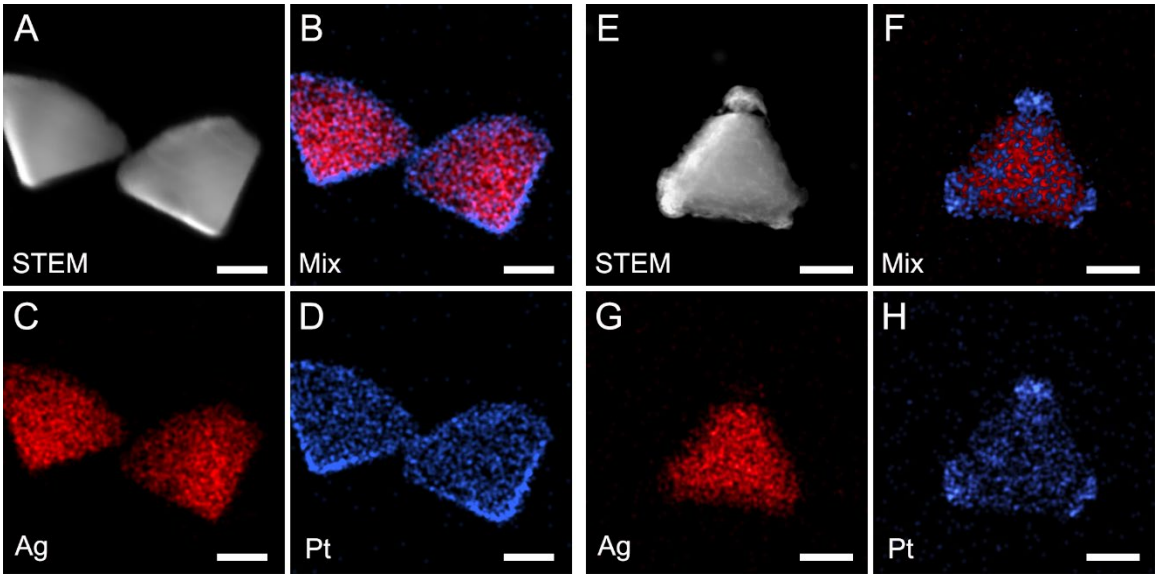

Figure 2. Scanning transmission electron microscopy energy dispersive x-ray spectroscopy (STEM-EDS) images and elemental maps of Ag-Pt hybrids with a uniform Pt shell (A-D) and a Pt shell with significant tip protrusions (E-H). Scale bars: (A-D) 40 nm and (E-H) 30 nm.

The localization of Pt deposition on the Ag bipyramid cores is dependent on the kinetics of Pt deposition. The rate and amount of Pt deposited can be tuned by modifying the concentration of citrate and Pt^{2+}, as well as by changing the excitation wavelength and intensity (Figures 1 and 2). At moderate reaction rates (23.8 μM Pt^{2+}, 4.76 mM citrate), a thin, rough shell of Pt is deposited on the Ag bipyramid cores under this low-intensity visible light illumination (Figures 1A, 2A-D, and S3A). With an increased initial Pt concentration (71.4 μM Pt^{2+}, 4.76 mM citrate) or when the reaction time is extended (up to 20 hours), a thicker coating of Pt is deposited, with formation of spherical lobes at the tips of the bipyramids (Figures 1B, 2E-H, and S3B). Notably, under slower rates of Pt deposition (47.6 μM Pt^{2+}, 0.95 mM citrate), Pt deposition can be selectively localized at the tips of the Ag bipyramids (Figures 1C and S3C). Under kinetically slow reaction conditions, metal deposition preferentially occurs at the highest energy sites, which in this case are the tips of the bipyramids due to their high surface curvature and the presence of planar twin defects in the core bipyramids. This localization of Pt at areas of high electric field density has applications in the development of core-satellite bimetallic photochemical catalysts.[34, 35]

Under conditions where the concentration of citrate and the illumination wavelength and intensity are held constant, the amount of Pt deposited on the Ag bipyramid cores increases approximately linearly with the concentration of Pt^{2+} in solution (Figures S2B and S4). This, in turn, leads to a tunable and gradual redshift of the LSPR maximum of the Ag-Pt hybrid nanoparticles (Figure S2C). The intensity of the LSPR maximum does decrease somewhat with increasing platinum coverage but, importantly, it does not disappear even at high Pt coverages (Figure S2D). The retention of LSPR intensity in the visible region is key to the use of hybrid materials composed of a combination of plasmonic metals (such as Ag) and poorly plasmonic metals (such as Pt) in plasmonic applications. The formation of Ag core-Pt shell structures, as opposed to removal of the Ag core via galvanic replacement, is likely a key factor in the maintenance of plasmonic properties in the Ag-Pt hybrid nanostructures. The LSPR of the three different Ag-Pt particle morphologies likewise red-shifts with increasing Pt coverage at the tips. The core-shell particles (Figure 1A) have the least shifted LSPR while the particles with both a thick shell and tip protrusions (Figure 1B) have a significantly red-shifted LSPR (Figure 3).

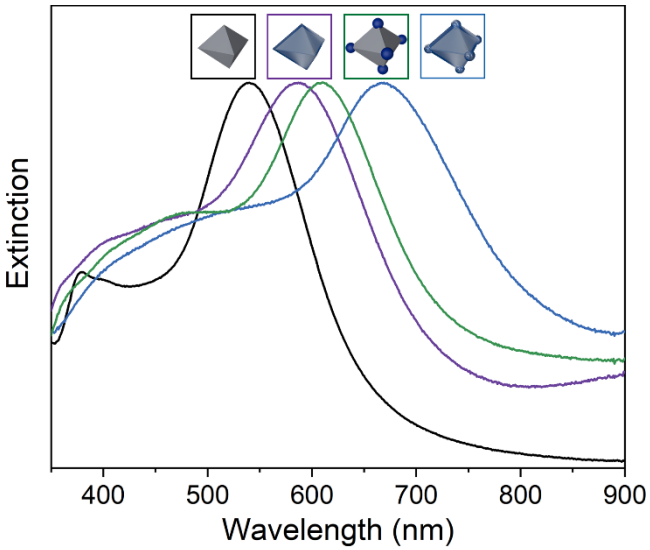

Figure 3. Normalized UV-visible spectra of Ag bipyramids and different Ag-Pt particle morphologies: core-shell, core-satellite, and core with shell and spherical lobes.

Plasmon-mediated chemical reactions have a series of characteristics that distinguish them from more common thermal reactions as well as from reactions driven by plasmon-induced photothermal heating. These characteristics include: (1) a reaction rate that trends with the LSPR spectrum of the nanoparticle being excited; (2) a linear dependence of reaction rate on illumination intensity; and (3) a lack

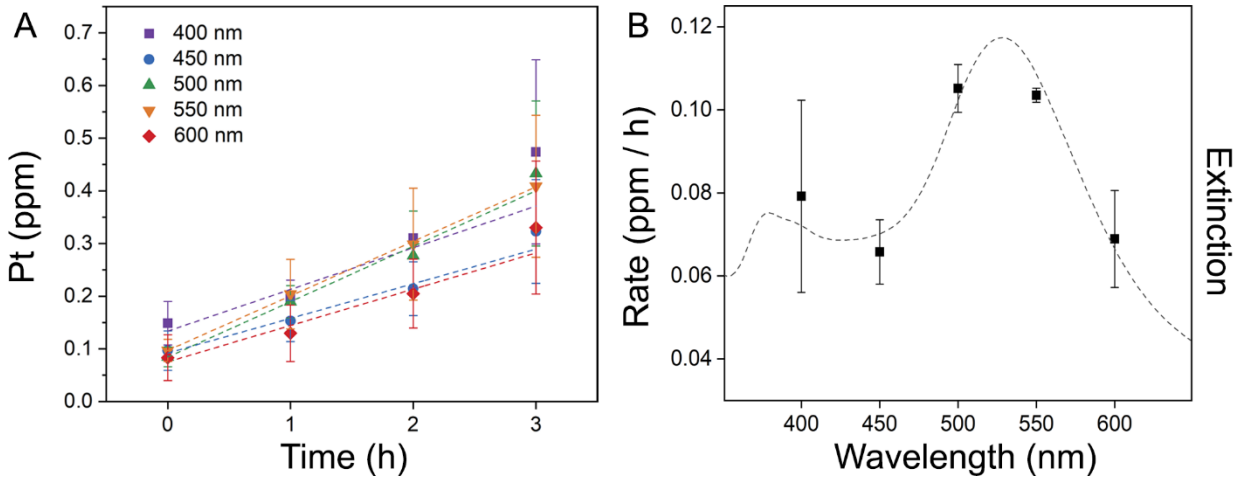

Figure 4. Wavelength dependence of Pt deposition rate during Ag-Pt hybrid particle formation. (A) Plot of the amount of Pt deposited onto Ag triangular bipyramids over time under different illumination wavelengths from 400 to 600 nm (all at 0.03 W). (B) Plot of reaction rate vs. wavelength, showing a correspondence between Pt deposition rate and the LSPR of the Ag bipyramid cores. Rates in (B) were estimated from a linear fit of the data in (A). Pt content was measured using inductively coupled plasma mass spectrometry (ICP-MS).

of reaction, or reduced reaction rate, in the absence of illumination.[36] In addition, citrate becomes a significantly more effective reducing agent at elevated temperatures—it is commonly used at or near reflux during the synthesis of noble metal nanoparticles[37-39]—and therefore contributions from overall solution heating under illumination must be isolated or excluded.

To probe the wavelength dependence of Pt deposition, growth solutions of constant chemical composition (23.8 μM Pt^{2+} and 4.76 mM citrate) were illuminated at wavelengths of 400, 450, 500, 550, and 600 nm (all ± 20 nm) at a constant intensity of 0.03 W. The citrate concentration was selected to be in significant excess, and a moderate Pt^{2+} concentration was chosen to ensure a sufficient reaction rate to be differential but also to limit the possibility of galvanic replacement from a high concentration of excess Pt ions. The illumination intensity of 0.03 W is the maximum intensity possible with the 150 W halogen lamp light source and the 400 ± 20 nm bandpass filter. Samples were taken from the reactions at one-hour intervals and immediately centrifuged and washed to remove unreacted Pt ions. The isolated nanoparticles were then dissolved in aqua regia and analyzed by inductively coupled plasma mass spectrometry (ICP-MS) to quantify the amount of Pt deposited onto the Ag nanoparticle cores (Figure 4A and S5). The final product at three hours under each condition was also imaged via scanning electron microscopy (SEM) (Figure S6).

The Pt deposition rate at each wavelength was estimated using a linear fit of the data from these time course Pt deposition experiments (Figure 4A). A plot of the Pt deposition rate at each wavelength versus the extinction spectrum of the initial Ag bipyramid cores (Figure 4B) shows a strong correspondence between rate and the LSPR intensity. Illumination at 500 and 550 nm, on either side of the longitudinal LSPR maximum of the Ag bipyramids, yields the highest reaction rate, while the rate is slower at the absorbance minima (450 and 600 nm). The second peak in the extinction spectrum—at approximately 375 nm—corresponds to the transverse plasmon resonance of the Ag bipyramids[33] and, consequently, the rate increases slightly under 400 nm illumination relative to the rate at 450 nm. This strong trend of Pt deposition rate with the extinction spectrum of the Ag bipyramids supports a plasmon-mediated reduction mechanism.

Using the same chemical reaction conditions and ICP-MS kinetics technique described above, the intensity dependence of Pt reduction rate was evaluated using a constant wavelength of 550 nm with an illumination power gradient of 0.03, 0.05, 0.10, 0.15, and 0.20 W (Figure 5A, S7, and S8). These values correspond to power densities of 5, 8, 15, 23, and 31 mW/cm^2, respectively (Table S1). Plasmonic excitation can lead to localized heat increases at the nanoparticle surface, known as photothermal heating.[40] Chemical processes that are driven by photothermal heating exhibit an exponential increase in rate with increasing illumination intensity.[36] In contrast, the rate of Pt deposition on the Ag bipyramids exhibits a linear dependence on intensity at low intensities and a sublinear dependence at higher intensities (Figure 5B). This is consistent with a slow, rate-limiting plasmon-mediated process at low intensities and a mass transport limited process at higher intensities. Wu *et al.* observed similar behavior for the plasmon-mediated synthesis of Ag triangular nanoprisms and proposed that at low intensities the plasmon-assisted oxidation of citrate is rate-determining, while at higher intensities—and therefore faster rates of citrate oxidation—the mass transport of Ag^+ ions becomes limiting due to their low concentration in solution.[26] The concentration of Pt^{2+} ions in the current synthesis is likewise low, and it is likely that an analogous effect is responsible for the observed linear to sublinear trend.

When a growth solution with the same chemical composition is left in the dark at room temperature (22 °C) for three hours, there is a small amount of Pt deposition, but it is significantly lower than what is observed under standard illumination conditions (550 nm, 0.1W) (Figure 6 and S9A). The thermal reduction of Pt^{2+} is thermodynamically

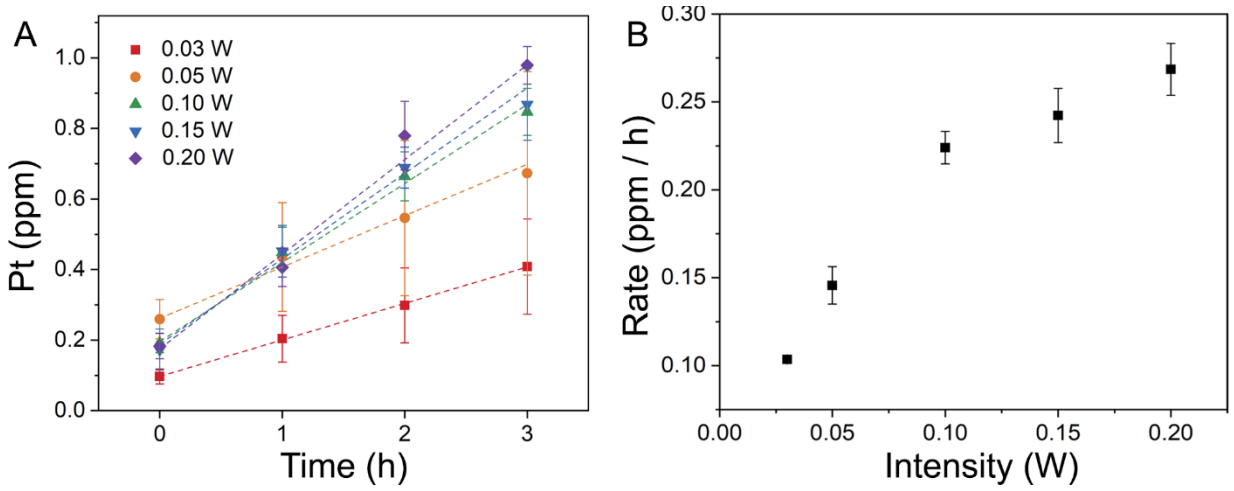

Figure 5. Intensity dependence of Pt deposition rate during Ag-Pt hybrid particle formation. (A) Plot of the amount of Pt deposited onto Ag triangular bipyramids over time under different illumination powers from 0.03 to 0.2 W (all at 550 nm). (B) Plot of reaction rate vs. intensity, showing a linear to sublinear dependence of Pt deposition rate on light intensity. Rates in (B) were estimated from a linear fit of the data in (A). Pt content was measured using ICP-MS.

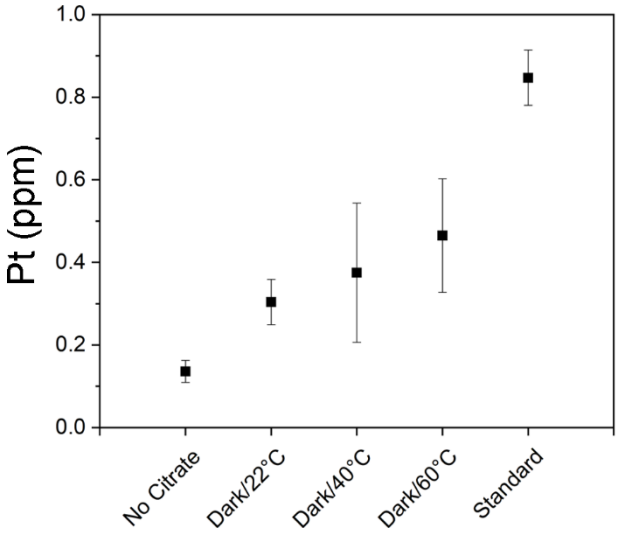

Figure 6. Quantification of the amount of Pt deposited onto Ag triangular bipyramids after three hours under various control conditions compared to standard chemical and illumination conditions. Pt content was measured using ICP-MS.

allowed, so it is possible that some thermal reduction occurs in the dark. It is also possible that in the absence of significant plasmon-assisted reduction of Pt^{2+} by citrate, galvanic replacement becomes more predominant. However, an illuminated reaction solution with only Pt^{2+} (no added citrate) shows negligible Pt deposition after three hours (Figure 6 and S10), so it is likely there is a small thermal reduction contribution, at least in the dark. The lack of Pt^{2+} deposition in the absence of the reducing agent sodium citrate also supports a classic plasmon-mediated redox cycle involving the hole-mediated oxidation of citrate and the subsequent reduction of Pt^{2+} by thermalized electrons.

When stored overnight—either under room light or in the dark—the Ag-Pt hybrid nanoparticles synthesized under standard illumination conditions change color slightly, indicating continued slow thermal Pt deposition. After a few days to a week, they have all become a teal color, which is typical of significant Pt deposition. However, when the particles are instead immediately centrifuged after three hours of synthesis and resuspended in water, they remain stable for at least a month without any observable color change (Figure S11). Both Pt^{2+} and citrate are in excess and are not used up in three hours of reaction, and therefore the presence of residual reactants results in continued Pt deposition via a non-plasmonic mechanism.

Illumination of the growth solution with the halogen lamp does cause some increase in the overall temperature of the reaction solution. For most reactions, the average solution temperature is in the range of approximately 30-40 °C after three hours, while for illumination at 550 nm and 0.2 W, the average temperature reaches a maximum of 47 °C (Table S2). Therefore, control reactions were conducted in the dark at 40 °C and at 60 °C, the latter of which is well above the temperature reached by any of the reaction conditions. In both cases, the amount of reduced Pt is significantly below what is observed at the standard 500 nm/0.1 W illumination—a condition which reaches an average temperature of 41 °C (Figure 6 and S9B,C). This shows that while increasing temperature does increase the rate of non-plasmonic processes—either thermal reduction or galvanic exchange—these thermal reactions are not responsible for the observed deposition under visible light illumination. In addition, a plot of reaction rate vs. final temperature diverges at high temperatures, again showing that the reactivity cannot be explained by heating (Figure S12).

As mentioned above, a reaction solution with no added citrate shows negligible Pt reduction after three hours, while in the presence of citrate and illumination significant, tunable Pt deposition occurs on the same timescale. However, this reaction without citrate does proceed slowly under illumination and, if the solution without added citrate is illuminated overnight (20 hours), tip deposition of Pt occurs onto the Ag bipyramid cores and the reaction solution becomes teal (Figure 7A and S13B). This selectivity to tip deposition is indicative of a kinetically slow process. Identical reaction solutions incubated at 22 °C or 40 °C overnight in

the dark showed no color change and no Pt deposition, confirming that this is a light-induced process (Figure S13A-D). In addition, a reaction solution without citrate remains stable in the dark for over a week but reacts slowly over the same period if left under room light, demonstrating that even very low intensity light is sufficient to drive this process (Figure S13E). It is important to note that there is likely a very small amount of residual citrate leftover from Ag bipyramid synthesis even in reactions without added citrate. To test the role of this residual citrate, the Ag bipyramids were washed once with water in addition to simply isolating them via centrifugation. These washed bipyramids were illuminated overnight with 23.8 μM Pt^{2+} in a total volume of 21 mL, identically to the "no citrate" control. The resulting solution turned a light teal and SEM images again show tip deposition, with some contrast that could potentially be due to galvanic replacement (Figure 7B). This suggests that growth in the presence of citrate proceeds via a process mediated by citrate oxidation, while a separate, very slow, direct hot electron reduction process and/or plasmon-induced galvanic replacement occurs in the absence of citrate. The significant difference in time scales between citrate-mediated Pt deposition (Figure 1) and direct reduction of Pt ions by hot electrons (Figure 7 and S10A) points to the inefficiency of the second process, which is highly localized to the tips of the Ag bipyramid cores by short carrier lifetimes.

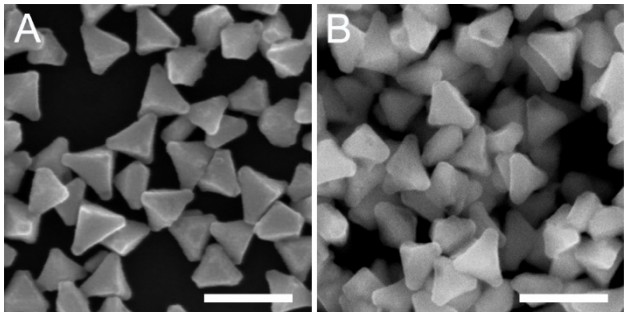

Figure 7. SEM images of Ag-Pt hybrid particles formed after twenty hours of illumination in the absence of citrate (Pt^{2+} only). The Ag bipyramid core particles in (A) were isolated via centrifugation according to the standard protocol before use while the Ag core particles in (B) were also washed once with water before use. Scale bars: 200 nm.

Evidence for Ag-Pt hybrid nanoparticle formation that is driven by thermalized electrons from citrate oxidation rather than its hole scavenger capabilities can be found in the Pt shell growth that takes place in the reactions with higher concentrations of citrate. Hot electrons have short lifetimes and therefore Pt deposition due to direct reduction by hot electrons would be expected to be localized at the areas of highest electric field density—the tips of the bipyramids. In contrast, work on citrate-mediated Ag deposition onto Au and Ag cores has shown that electrons produced via plasmon-enhanced oxidation of citrate have long lifetimes and therefore lead to the formation of core-shell structures rather than core-satellite structures.[25, 41]

To confirm the role of the Ag core, large Ag triangular nanoprisms with a LSPR maximum in the near infrared region (975 nm) were synthesized and then purified and illuminated under the same chemical and illumination conditions used for the other control experiments. Plasmon-mediated reduction of Pt^{2+} would be expected to be slow or non-existent on these nanostructures because their LSPR maximum is very red-shifted from the illumination wavelength of 550 nm (Figure S14). Indeed, SEM images of the large triangular nanoprisms after exposure to Pt deposition conditions show evidence of galvanic replacement (hollow feature formation) along with scalloped edges that likely result from oxidative etching of the core nanoprisms under illumination (Figure S15). Previous reports in the literature have shown that when monometallic Ag nanostructures have a plasmon resonance that is red-shifted from the excitation wavelength, they stop growing due to the lack of plasmon-assisted citrate oxidation to produce electrons for reduction.[33, 42] Without this illumination, oxidation by dissolved O_2 in aqueous solution can become predominant. In contrast, illumination of a purified solution of smaller triangular nanoprisms—which absorb at 550 nm—under the same conditions that led to selective tip deposition for the bipyramids (47.6 μM Pt^{2+}, 0.95 mM citrate, 550 nm/0.1 W excitation) results in Ag nanoprisms with Pt islands at their tips (Figures S14 and S16). This confirms that plasmonic excitation of the Ag core is key to hybrid Ag-Pt nanostructure formation and shows that the plasmon-mediated deposition of Pt facilitated by citrate is extendable to other Ag core shapes as well, highlighting the versatility of the approach.

Conclusions

The plasmon-assisted oxidation of citrate described herein provides a powerful tool for achieving controlled Pt ion reduction kinetics in range that is inaccessible using thermal reduction and chemical parameters alone. In turn, this fine degree of kinetic control enables the selective deposition of a poorly plasmonic metal, Pt, at the tips of polyhedral plasmonic Ag cores. Importantly, this work expands the scope of citrate-assisted plasmon-mediated syntheses to metals other than Ag. Due to the broad use of citrate as a reducing agent for noble metals, we anticipate that this approach will be generalizable to other materials combinations and particle architectures.

ASSOCIATED CONTENT

Additional SEM images, ICP-MS data, photographs, UV-visible spectra, table of power density calculations, and table of average reaction temperatures. This material is available free of charge via the Internet at http://pubs.acs.org.

AUTHOR INFORMATION

Corresponding Author

* mpersonick@wesleyan.edu

Author Contributions

§ These authors contributed equally.

ACKNOWLEDGMENT

Acknowledgment is made to the U.S. Army Research Office for support of this research through a Young Investigator Program Award (W911NF-18-1-0156). This work was also supported by start-up funding from Wesleyan University. ICP-MS measurements were performed at the Yale Analytical and Stable Isotope Center (YASIC), a Yale Institute for Biospheric Studies (YIBS) research center. SEM imaging at Wesleyan University was supported by the National Science Foundation Major Research

Instrumentation program under Grant No. 1725491. STEM imaging and additional SEM characterization was carried out at Yale University at The Yale Institute for Nanoscience and Quantum Engineering (YINQE).

REFERENCES

1. Robertson, D. D.; Personick, M. L. Growing Nanoscale Model Surfaces to Enable Correlation of Catalytic Behavior Across Dissimilar Reaction Environments. *Chem. Mater.* **2019,** *31*, 1121-1141.

2. Jung, H.; King, M. E.; Personick, M. L. Strategic Synergy: Advances in the Shape Control of Bimetallic Nanoparticles with Dilute Alloyed Surfaces. *Curr. Opin. Colloid Interface Sci.* **2019,** *40*, 104-117.

3. Gu, J.; Zhang, Y.-W.; Tao, F. Shape Control of Bimetallic Nanocatalysts through Well-Designed Colloidal Chemistry Approaches. *Chem. Soc. Rev.* **2012,** *41*, 8050-8065.

4. Straney, P. J.; Marbella, L. E.; Andolina, C. M.; Nuhfer, N. T.; Millstone, J. E. Decoupling Mechanisms of Platinum Deposition on Colloidal Gold Nanoparticle Substrates. *J. Am. Chem. Soc.* **2014,** *136*, 7873-7876.

5. Fennell, J.; He, D.; Tanyi, A. M.; Logsdail, A. J.; Johnston, R. L.; Li, Z. Y.; Horswell, S. L. A Selective Blocking Method to Control the Overgrowth of Pt on Au Nanorods. *J. Am. Chem. Soc.* **2013,** *135*, 6554-6561.

6. Yang, S.; Park, N.-Y.; Han, J. W.; Kim, C.; Lee, S.-C.; Lee, H. A Distinct Platinum Growth Mode on Shaped Gold Nanocrystals. *Chem. Commun.* **2012,** *48*, 257-259.

7. Alinezhad, A.; Gloag, L.; Benedetti, T. M.; Cheong, S.; Webster, R. F.; Roelsgaard, M.; Iversen, B. B.; Schuhmann, W.; Gooding, J. J.; Tilley, R. D. Direct Growth of Highly Strained Pt Islands on Branched Ni Nanoparticles for Improved Hydrogen Evolution Reaction Activity. *J. Am. Chem. Soc.* **2019,** *141*, 16202-16207.

8. King, M. E.; Personick, M. L. Iodide-Induced Differential Control of Metal Ion Reduction Rates: Synthesis of Terraced Palladium–Copper Nanoparticles with Dilute Bimetallic Surfaces. *J. Mater. Chem. A* **2018,** *6*, 22179-22188.

9. Weiner, R. G.; Kunz, M. R.; Skrabalak, S. E. Seeding a New Kind of Garden: Synthesis of Architecturally Defined Multimetallic Nanostructures by Seed-Mediated Co-Reduction. *Acc. Chem. Res.* **2015,** *48*, 2688-2695.

10. Stone, A. L.; King, M. E.; McDarby, S. P.; Robertson, D. D.; Personick, M. L. Synthetic Routes to Shaped AuPt Core–Shell Particles with Smooth Surfaces Based on Design Rules for Au Nanoparticle Growth. *Part. Part. Syst. Charact.* **2018,** *35*, 1700401.

11. Xia, X.; Wang, Y.; Ruditskiy, A.; Xia, Y. 25th Anniversary Article: Galvanic Replacement: A Simple and Versatile Route to Hollow Nanostructures with Tunable and Well-Controlled Properties. *Adv. Mater.* **2013,** *25*, 6313-6333.

12. Chen, J.; Wiley, B.; McLellan, J.; Xiong, Y.; Li, Z.-Y.; Xia, Y. Optical Properties of Pd–Ag and Pt–Ag Nanoboxes Synthesized via Galvanic Replacement Reactions. *Nano. Lett.* **2005,** *5*, 2058-2062.

13. Sun, Y.; Xia, Y. Shape-Controlled Synthesis of Gold and Silver Nanoparticles. *Science* **2002,** *298*, 2176-2179.

14. González, E.; Arbiol, J.; Puntes, V. F. Carving at the Nanoscale: Sequential Galvanic Exchange and Kirkendall Growth at Room Temperature. *Science* **2011,** *334*, 1377-1380.

15. Jing, H.; Wang, H. Structural Evolution of Ag–Pd Bimetallic Nanoparticles through Controlled Galvanic Replacement: Effects of Mild Reducing Agents. *Chem. Mater.* **2015,** *27*, 2172-2180.

16. Yu, Y.; Zhang, Q.; Yao, Q.; Xie, J.; Lee, J. Y. Guiding Principles in the Galvanic Replacement Reaction of an Underpotentially Deposited Metal Layer for Site-Selective Deposition and Shape and Size Control of Satellite Nanocrystals. *Chem. Mater.* **2013,** *25*, 4746-4756.

17. Bi, C.; Song, Y.; He, H.; Wu, C.; Du, W.; Huang, L.; Moehwald, H.; Xia, H. Simple Synthesis and Surface Facet-Tuning of Ultrathin Alloy-Shells of Au@AuPd Nanoparticles via Silver-Assisted Co-Reduction onto Facet-Controlled Au Nanoparticles. *J. Mater. Chem. A* **2018,** *6*, 7675-7685.

18. Gilroy, K. D.; Yang, X.; Xie, S.; Zhao, M.; Qin, D.; Xia, Y. Shape-Controlled Synthesis of Colloidal Metal Nanocrystals by Replicating the Surface Atomic Structure on the Seed. *Adv. Mater.* **2018,** *30*, 1706312.

19. Wu, Y.; Sun, X.; Yang, Y.; Li, J.; Zhang, Y.; Qin, D. Enriching Silver Nanocrystals with a Second Noble Metal. *Acc. Chem. Res.* **2017,** *50*, 1774-1784.

20. Straney, P. J.; Diemler, N. A.; Smith, A. M.; Eddinger, Z. E.; Gilliam, M. S.; Millstone, J. E. Ligand-Mediated Deposition of Noble Metals at Nanoparticle Plasmonic Hotspots. *Langmuir* **2018,** *34*, 1084-1091.

21. Lou, Z.; Fujitsuka, M.; Majima, T. Pt–Au Triangular Nanoprisms with Strong Dipole Plasmon Resonance for Hydrogen Generation Studied by Single-Particle Spectroscopy. *ACS Nano* **2016,** *10*, 6299-6305.

22. Zhang, J.; Langille, M. R.; Mirkin, C. A. Photomediated Synthesis of Silver Triangular Bipyramids and Prisms: The Effect of pH and BSPP. *J. Am. Chem. Soc.* **2010,** *132*, 12502-12510.

23. Langille, M. R.; Personick, M. L.; Mirkin, C. A. Plasmon-Mediated Syntheses of Metallic Nanostructures. *Angew. Chem. Int. Ed.* **2013,** *52*, 13910-13940.

24. Jin, R.; Cao, Y.; Mirkin, C. A.; Kelly, K. L.; Schatz, G. C.; Zheng, J. G. Photoinduced Conversion of Silver Nanospheres to Nanoprisms. *Science* **2001,** *294*, 1901-1903.

25. Redmond, P. L.; Wu, X.; Brus, L. Photovoltage and Photocatalyzed Growth in Citrate-Stabilized Colloidal Silver Nanocrystals. *J. Phys. Chem. C* **2007,** *111*, 8942-8947.

26. Wu, X.; Redmond, P. L.; Liu, H.; Chen, Y.; Steigerwald, M.; Brus, L. Photovoltage Mechanism for Room Light Conversion of Citrate Stabilized Silver Nanocrystal Seeds to Large Nanoprisms. *J. Am. Chem. Soc.* **2008,** *130*, 9500-9506.

27. Zhai, Y.; DuChene, J. S.; Wang, Y.-C.; Qiu, J.; Johnston-Peck, A. C.; You, B.; Guo, W.; DiCiaccio, B.; Qian, K.; Zhao, E. W.; et al. Polyvinylpyrrolidone-Induced Anisotropic Growth of Gold Nanoprisms in Plasmon-Driven Synthesis. *Nat. Mater.* **2016,** 1*5*, 889-895.

28. Golze, S. D.; Hughes, R. A.; Rouvimov, S.; Neal, R. D.; Demille, T. B.; Neretina, S. Plasmon-Mediated Synthesis of Periodic Arrays of Gold Nanoplates Using Substrate-Immobilized Seeds Lined with Planar Defects. *Nano. Lett.* **2019,** *19*, 5653-5660.

29. Forcherio, G. T.; Baker, D. R.; Boltersdorf, J.; Leff, A. C.; McClure, J. P.; Grew, K. N.; Lundgren, C. A. Targeted Deposition of Platinum onto Gold Nanorods by Plasmonic Hot Electrons. *J. Phys. Chem. C* **2018,** *122*, 28901-28909.

30. Ortiz, N.; Zoellner, B.; Hong, S. J.; Ji, Y.; Wang, T.; Liu, Y.; Maggard, P. A.; Wang, G. Harnessing Hot Electrons from Near IR Light for Hydrogen Production Using Pt-End-Capped-AuNRs. *ACS Appl. Mater. Interfaces* **2017,** *9*, 25962-25969.

31. Kontoleta, E.; Askes, S. H. C.; Garnett, E. C. Self-Optimized Catalysts: Hot-Electron Driven Photosynthesis of Catalytic Photocathodes. *ACS Appl. Mater. Interfaces* **2019**, *11*, 35713-35719.

32. Aslam, U.; Linic, S. Kinetic Trapping of Immiscible Metal Atoms into Bimetallic Nanoparticles through Plasmonic Visible Light-Mediated Reduction of a Bimetallic Oxide Precursor: Case Study of Ag–Pt Nanoparticle Synthesis. *Chem. Mater.* **2016,** *28*, 8289-8295.

33. Zhang, J.; Li, S.; Wu, J.; Schatz, G. C.; Mirkin, C. A. Plasmon-Mediated Synthesis of Silver Triangular Bipyramids. *Angew. Chem. Int. Ed.* **2009,** *48*, 7787-7791.

34. Zheng, Z.; Tachikawa, T.; Majima, T. Single-Particle Study of Pt-modified Au Nanorods for Plasmon-Enhanced Hydrogen Generation in Visible to Near-Infrared Region. *J. Am. Chem. Soc.* **2014,** *136*, 6870-6873.

35. Wang, F.; Li, C.; Chen, H.; Jiang, R.; Sun, L.-D.; Li, Q.; Wang, J.; Yu, J. C.; Yan, C.-H. Plasmonic Harvesting of Light Energy for Suzuki Coupling Reactions. *J. Am. Chem. Soc.* **2013,** *135*, 5588-5601.

36. Christopher, P.; Xin, H.; Marimuthu, A.; Linic, S. Singular Characteristics and Unique Chemical Bond Activation Mechanisms of Photocatalytic Reactions on Plasmonic Nanostructures. *Nat. Mater.* **2012,** *11*, 1044-1050.

37. Harriman, A.; Millward, G. R.; Neta, P.; Richoux, M. C.; Thomas, J. M. Interfacial Electron-Transfer Reactions between Platinum Colloids and Reducing Radicals in Aqueous Solution. *J. Phys. Chem.* **1988,** *92*, 1286-1290.

38. Furlong, D. N.; Launikonis, A.; Sasse, W. H. F.; Sanders, J. V. Colloidal Platinum Sols. Preparation, Characterization and Stability towards Salt. *J. Chem. Soc., Faraday Trans. 1* **1984,** *80*, 571-588.

39. Kimling, J.; Maier, M.; Okenve, B.; Kotaidis, V.; Ballot, H.; Plech, A. Turkevich Method for Gold Nanoparticle Synthesis Revisited. *J. Phys. Chem. B* **2006,** *110*, 15700-15707.

40. Qiu, J.; Wei, W. D. Surface Plasmon-Mediated Photothermal Chemistry. *J. Phys. Chem. C* **2014,** *118*, 20735-20749.

41. Xue, C.; Millstone, J. E.; Li, S.; Mirkin, C. A. Plasmon-Driven Synthesis of Triangular Core–Shell Nanoprisms from Gold Seeds. *Angew. Chem. Int. Ed.* **2007,** *46*, 8436-8439.

42. Xue, C.; Mirkin, C. A. pH-Switchable Silver Nanoprism Growth Pathways. *Angew. Chem. Int. Ed.* **2007,** *46*, 2036-2038.

TOC Graphic